Prediction of Viscosity−Temperature−Composition Surfaces in a Single Expression for Methanol−Water and Acetonitrile−Water Mixtures

Anita M. Katti,*,† Nicoleta E. Tarfulea,‡ Corey J. Hopper,† and Kraig R. Kmiotek†

Department of Chemistry and Physics, and Department of Mathematics, Purdue University Calumet, Hammond, Indiana

The modeling of the surface of viscosity in composition and temperature at atmospheric pressure for methanol−water and acetonitrile−water was performed by interconnecting various elementary functions and testing them in a systematic manner to minimize the least-squares error. The systematic approach involved developing expressions that were the sum or product of elementary functions in temperature and composition, then visually observing their fit and quantitating the error. To reduce the error, transformation of the data using elementary functions was necessary to create a modified surface simpler in form. For MeOH−H_2O, the least-squares error was 0.6 and 0.01 for untransformed data and transformed data, respectively. Similarly, for ACN−H_2O, the error was 0.3 and 0.008 for untransformed and transformed data, respectively. The expression describing the viscosity−composition−temperature relationship for both the transformed and untransformed data was a quadratic in x with exponential functions of T as coefficients where $T°$ is a nondimensionalizing term of value one. The transformed temperature is $\log(T/T°) + 2$, while the transformed viscosity was $\eta^{1/8}$.

Introduction

In reversed-phase chromatography, the common mobile phase modifiers are acetonitrile and methanol where variations in temperature and composition affect the production rate and yield at the process scale.[1] In process chromatography, a maximum design pressure is defined for the column, piping, and other equipment so that leaking, cracking, or bursting is avoided at the operating pressure.[2−4] Furthermore, defining pressure limits avoid warping of the column or tubing.[5] Control of the temperature and feed concentration can avoid changes in viscosity that may result in viscous fingering,[6] poor separation, and higher operating pressures. The robustness[7] of the process is altered by variations in the operating pressure which causes variability in the column efficiency,[8] fluctuations in the adsorption isotherm,[9] and performance of the separation.[10,11] Creating an engineering design and operating conditions that scale-up to meet yield and production rate[12,13] targets are critical to effective strategies for marketing, sales, and profitability. Applications of process chromatography show that in low, medium, and high pressure modes, there is an interconnection between the design pressure, the operating parameters, and the outcome of optimization protocols.[14−17]

In the economic modeling of process chromatography, it has been shown that the maximum of the objective function (e.g., $\$\cdot kg^{-1}$, Production Rate, Yield·Production Rate, Specific Production) occurs at the maximum design pressure under isocratic and gradient conditions.[18,19] Chromatography unit operations have inherent limits in their design pressure because of the impact of the construction material costs to fabricate a column, pump, packing media, and other tools including piping, fittings, and devices.[20,21] Furthermore, safety systems such as rupture discs, spring relief, and pump relief are specified in accordance to the design and the process operating pressure.[22]

In ion-exchange and hydrophobic interaction chromatography, viscosity is a function of the salt concentration. In supercritical fluid chromatography, the viscosity changes with the operating pressure due to the compression of the mobile phase and has subsequent effects on temperature.[1,23,24] In reversed-phase and normal-phase chromatography, the mobile phase modifier is a nonlinear function of temperature and composition and at very high pressures induces a radial temperature distribution.[1,25] The modeling of viscosity as a function of temperature is commonly investigated using the analogous Antoine equation.[26] Correlations for pure methanol have been developed as a function of pressure,[27,28] and new technologies matured for measurement of viscosity.[29]

Binary mixtures of viscosity have been modeled using the weighted sum of the natural logarithm of the pure component viscosities,[30] sometimes including an excess[31] term. For polar methanol mixtures, Li and Carr[32] have used the Lobe Correlation,[26] Domínguez[33] has used the UNIFAC model, and Teja and Rice have used the corresponding states method[34] to predict viscosity as a function of composition at specific values of the temperature. Similarly, the viscosity of acetonitrile has been measured[35] for mixtures.

Methanol−water (MeOH−H_2O) and acetonitrile−water (ACN−H_2O) mixtures exhibit a volume reduction upon mixing, due to solvation of the alcohol with water; thus, the increased size leads to a maximum in the viscosity composition curve. Heráez[36] found that the value of the maximum viscosity and the composition at the maximum viscosity increase with increasing carbon number. An extensive review of viscosity in terms of measurement methods, theory, and values of model coefficients for many solvent systems has been reported by Viswanath.[37]

To perform design calculations for pressure, use of a simple, continuous analytical function is necessary, eq 1: length (L),

* To whom correspondence should be addressed. E-mail: katti@calumet.purdue.edu.
† Department of Chemistry and Physics.
‡ Department of Mathematics.

10.1021/je800607j CCC: $40.75
Published on Web 11/06/2008

Table 1. Raw Viscosity Data by Digitization

	Viscosity, η/cP										
	% MeOH										
	100	90	80	70	60	50	40	30	20	10	0
	% H_2O										
T/K	0	10	20	30	40	50	60	70	80	90	100
288.15	0.63	1.05	1.40	1.69	1.91	2.02	2.0	1.92	1.72	1.43	1.10
293.15	0.60	0.93	1.25	1.52	1.72	1.83	1.83	1.75	1.57	1.32	1.00
298.15	0.56	0.84	1.12	1.36	1.54	1.62	1.62	1.56	1.40	1.18	0.89
303.15	0.51	0.76	1.01	1.21	1.36	1.43	1.43	1.36	1.23	1.04	0.79
308.15	0.46	0.69	0.91	1.09	1.21	1.26	1.24	1.19	1.07	0.92	0.70
313.15	0.42	0.64	0.83	0.98	1.08	1.12	1.11	1.05	0.96	0.82	0.64
318.15	0.39	0.58	0.76	0.89	0.98	1.02	1.00	0.96	0.87	0.75	0.58
323.15	0.37	0.54	0.70	0.82	0.90	0.94	0.93	0.89	0.82	0.71	0.54
328.15	0.36	0.50	0.65	0.76	0.84	0.88	0.88	0.84	0.77	0.67	0.51
333.15	0.33	0.47	0.61	0.72	0.79	0.81	0.81	0.77	0.70	0.61	0.47
	% ACN										
T/K	100	90	80	70	60	50	40	30	20	10	0
293.15	0.40	0.54	0.70	0.81	0.89	0.98	1.09	1.30	1.23	1.17	1.10
298.15	0.37	0.50	0.56	0.69	0.81	0.90	0.99	1.13	1.10	1.05[a]	1.00
303.15	0.35	0.46	0.52	0.59	0.72	0.82	0.89	0.98	0.98	0.94[a]	0.89
308.15	0.32	0.43	0.45	0.52	0.65	0.74	0.80	0.86	0.87	0.83[a]	0.79
313.15	0.30	0.39	0.43	0.47	0.59	0.68	0.72	0.76	0.78	0.74[a]	0.70
318.15	0.27	0.36	0.41	0.44	0.54	0.62	0.65	0.68	0.70	0.67[a]	0.64
323.15	0.25	0.33	0.38	0.43	0.50	0.58	0.59	0.61	0.64	0.61[a]	0.58
328.15	0.24	0.31	0.36	0.41	0.46	0.53	0.55	0.57	0.60	0.57[a]	0.54
333.15	0.23	0.29	0.34	0.38	0.43	0.49	0.51	0.53	0.56	0.54	0.51
273.15	0.22	0.27	0.31	0.35	0.41	0.46	0.49	0.50	0.53	0.50	0.47

[a] Interpolated value of scanned data.

linear velocity (u), where $u = L/t_o$, with t_o as the void time, viscosity (η), temperature (T), permeability constant (k_o = 0.001), and particle size (d_p)(where $T = T/T°$ and $\eta = \eta/\eta°$). Since viscosity is a function of temperature (T) and composition (x), it is necessary to determine a functional form of this surface, $\eta(x,T)$.[38] Development of such a function enables design calculations for decision making, such as the need for temperature control due to viscosity variations and for facilitating safety analysis regarding pressure fluctuations.

$$\Delta P = \frac{1}{k_o} \cdot \frac{u \cdot L \cdot \eta(x,T)}{d_p^2} \quad (1)$$

This paper applies an empirical yet systematic approach to ascertain a quantitative function for the MeOH−H_2O and ACN−H_2O viscosity surface having a minimum least-squares error with respect to the experimental data. This is performed by transformation of the surface $\eta(x,T)$ by mapping the coordinates to create a new function $\hat{\eta}(x,\hat{T})$ that is simpler in appearance.[39] For example, rectilinear coordinates are transformed to curvilinear coordinates to create a natural system for mathematical analysis.[40] This paper investigated many transformations to map the MeOH−H_2O and ACN−H_2O surfaces into a shape having a mathematical expression that aligns with the experimental data.[41] This applied an iterative approach involving observing the shape of the surface relative to the experimental data and iterating with elementary functions.

Experimental

An HP-1090 with Chemstation software (GMI Analytical, Ramsey, MN, USA) was used to measure the pressure drop as a function of the methanol and acetonitrile (HPLC grade, Mallinckrodt, St. Louis, MO, USA) concentration. Methanol measurements were performed on a Daiso 4.6 mm × 50 mm, SP-ODS-A, 5 μm, 120 Å, and acetonitrile measurements on Daiso 4.6 mm × 50 mm BIO, 10 μm, 200 Å (Santa Clara, CA, USA). Viscosity raw data[42] were digitized (Un-Scan-It Orem, UT, USA).

Discussion of Results

This paper analyzes the MeOH−H_2O and ACN−H_2O surface viscosity function in composition and temperature in four ways: (I) Apply pure component viscosity data as a function of temperature by traditional functions (e.g., Antoine equation). (II) Evaluate and model MeOH−H_2O and ACN−H_2O viscosity data as a function of composition and temperature. (III) Evaluate and model MeOH−H_2O and ACN−H_2O viscosity data by various transformations to further reduce the least-squares error. (IV) Application of square plots to evaluate the measured and calculated viscosity, effective particle size, and pressure.

I. Antoine-Type Functions: Pure Component Data for MeOH and ACN. The Antoine type equation for vapor pressure is the classical form for evaluating the pure component solvent viscosity as a function of temperature. This equation advanced simpler equations, Table 1, for modeling viscosity−temperature relationships for polar molecules. Published data are compared with those obtained using the Nelder−Mead simplex routine[43] modified by Tarfulea in this paper. The reductions observed in the error are likely due to the improvements in the mathematical and computer methods as well as experimental viscosity data obtained by improved techniques.

Figure 1 shows the Antoine equation fit to the experimental data for methanol and acetonitrile as a function of temperature via the Tarfulea method. The errors are of the order 0.001.

II. Untransformed Functions: Viscosity Surface, Composition, and Temperature. Figure 2 illustrates the MeOH−H_2O and ACN−H_2O surface plots for the experimental viscosity data in composition and temperature. The difficulty of modeling this

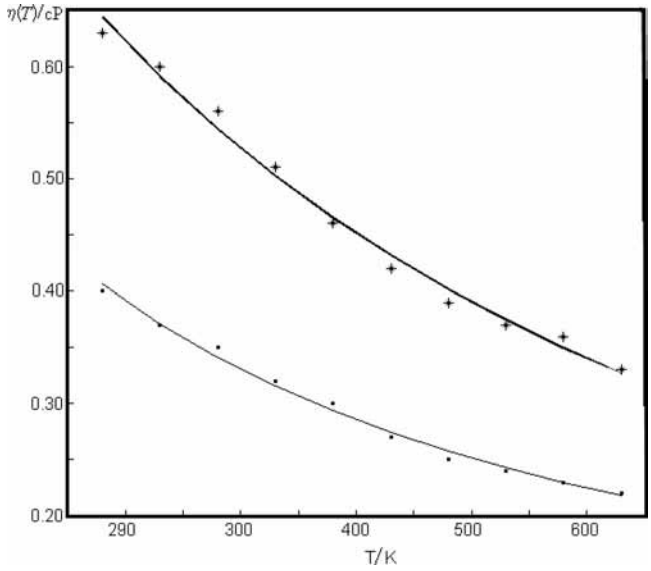

Figure 1. Viscosity of methanol and acetonitrile using the Antoine equation via the Tarfulea method. ■, Acetonitrile data; *, methanol data; −, fitted curve.

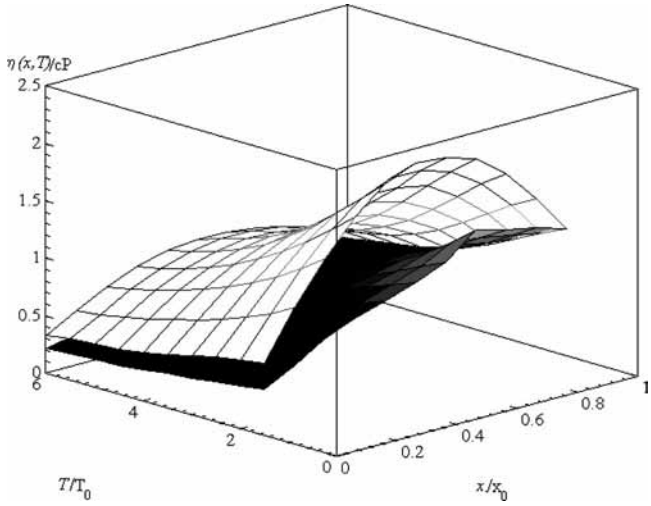

Figure 2. Viscosity, composition, and temperature surface for ACN−H_2O and MeOH−H_2O (□, MeOH; ■, ACN) where $T_o = 10$ and $x_o = 100$.

surface rests in the lack of a plane or an axis of symmetry. Acetonitrile exhibits less curvature than methanol in aqueous solution.

The use of a quadratic polynomial, $Ax^2 + Bx + C$, to fit the MeOH−H_2O viscosity composition data at constant temperature gives curves with low error.[32] Figure 3 shows that when each of the coefficients A, B, and C of the isothermal quadratic functions for MeOH−H_2O is plotted against the temperature a quadratic relationship is obtained with correlation coefficient values greater than 0.998. This second degree order expression in the coefficients illustrates the reason for the large degree of nonlinearity for the MeOH−H_2O viscosity, $\eta(x,T)$.

The search for a smooth, continuous function $\eta(x,T)$ required a search for mathematical functions of composition and temperature to be applied in tandem to fit this surface. Fourier transformations on data are inherently irrelevant. Trigonometric transformations are not applicable, as this surface does not exhibit waves. The experimental data shown in Figure 2 exhibit an asymmetric knoll. Therefore, various two-dimensional functions (e.g., power, exponentials, and polynomials in x and T) were evaluated systematically as summations or products. Many

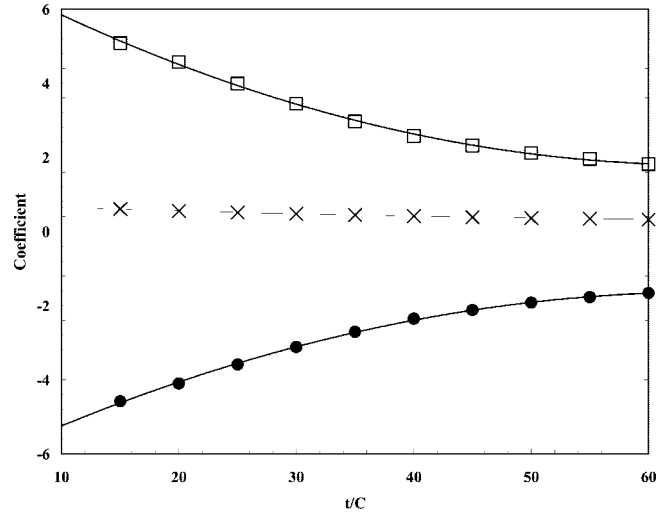

Figure 3. Quadratic equation coefficients A, B, and C as a function of temperature for MeOH−H_2O: ○, A; ×, B; □, C.

combinations of these functions were studied by visual inspection of the shape of the surface in conjunction with the data and the calculated value of the least-squares error. These observations led to suggestions of translation or modification or evaluation of new functions to improve the fit. This iterative process led to eqs 2 to 5, which illustrate a few examples of functions having a low error. Equation 2 is a quadratic expression in x with exponential functions of T as coefficients. Equation 3 is the product of a power function in T and a quadratic in x. Equation 4 is a summation function between a quadratic in both T and x. Similarly, eq 5 is a summation of an exponential in T and a quadratic in x.

$$\eta(x,T) = (a_1 e^{-a_2 T} + a_3)x^2 + (a_4 e^{-a_5 T} + a_6)x + (a_7 e^{-a_8 T} + a_9) \quad (2)$$

$$\eta(x,T) = a_o(T)^N(b_1 x^2 + b_2 x + b_3) \quad (3)$$

$$\eta(x,T) = a_1(T - a_2)^2 - b_1(x - b_2)^2 + c_1 \quad (4)$$

$$\eta(x,T) = a_o(a_1 e^{-a_2 T} + a_3) - b_1(x - b_2)^2 + c_1 \quad (5)$$

The least-squares errors for these surface functions for MeOH−H_2O and ACN−H_2O are summarized in Table 2. Equation 2 gives the lowest error for both MeOH−H_2O and ACN−H_2O, while for eqs 3 to 5 the least-squares error increases. Figures 4 and 5 illustrate the surface functions of MeOH−H_2O and ACN−H_2O, respectively, overlaid with the experimental surface. These figures show multiple intersections across surfaces. This nonlinear curvature limited the capacity to reduce the error, and thus an approach was taken to transform the experimental data. The methodology taken was in a similar vein as stated above.

III. Transformations: Viscosity as a Function of Composition and Temperature. To improve the error, transformations of the temperature and viscosity were made to reduce the total curvature of the surface or to create a surface that could be represented by elementary functions. The functions evaluated in addition to eqs 2 to 5 converted to transformed variables are eqs 6 to 9. Since the viscosity−composition form is quadratic in nature, x was not transformed.

$$\hat{\eta}(x,\hat{T}) = a_1 - a_2\hat{T} - a_4(x - a_3)^2 \quad (6)$$

$$\hat{\eta}(x,\hat{T}) = a_1 e^{a_2\hat{T}} + a_3 - a_4(x - a_5)^2 \quad (7)$$

Table 2. Summary of Measured Pressure Data

MeOH				ACN			
	%	flow rate	measured		%	flow rate	measured
t/°C	MeOH	Fv/ mL·min^{-1}	*P*/100 kPa[a]	*t*/°C	ACN	Fv/ mL·min^{-1}	*P*/100 kPa
40	0	0.1	4.8	40	0	0.1	2.6
40	0	1	49.5	40	0	0.5	13.1
40	0	2	98.0	40	0	1	26.2
40	0	3	150.3	40	0	2	52.4
40	0	4	204.8	40	0	2.5	65.5
40	20	0.1	4.5	40	0	3	78.6
40	20	1	64.3	40	0	3.5	91.7
40	20	2	130.5	40	20	0.1	2.6
40	20	3	196.5	40	20	0.5	6.0
40	20	4	268.5	40	20	1	26.4
40	40	0.1	8.5	40	20	2	59.8
40	40	1	78.8	40	20	2.5	71.8
40	40	2	161.5	40	20	3	83.8
40	40	3	246.0	40	20	3.5	100.8
40	40	4	307.0	40	40	0.1	2.66
40	60	0.1	8.5	40	40	0.5	12.4
40	60	1	77.3	40	40	1	26.4
40	60	2	154.8	40	40	2	51.8
40	60	3	234.3	40	40	2.5	66.4
40	60	4	306.3	40	40	3	80.8
40	80	0.1	8.3	40	40	3.5	92.8
40	80	1	58.8	40	60	0.1	2.4
40	80	2	122.3	40	60	0.5	11
40	80	3	191.8	40	60	1	23
40	80	4	261.8	40	60	2	44.2
40	100	0.1	6.0	40	60	2.5	54.6
40	100	1	36.0	40	60	3	68.8
40	100	2	76.3	40	60	3.5	76
40	100	3	122.0	40	80	0.1	1.5
40	100	4	172.8	40	80	0.5	8.4
60	0	0.1	4.8	40	80	1	16
60	0	1	44.0	40	80	2	34.4
60	0	2	92.3	40	80	2.5	44
60	0	3	142.5	40	80	3	49.2
60	0	4	194.3	40	80	3.5	59
60	20	0.1	4.5	40	100	0.1	1.1052
60	20	1	58.3	40	100	0.5	6
60	20	2	118.3	40	100	1	11.4
60	20	3	177.0	40	100	2	21.2
60	20	4	240.0	40	100	2.5	30
60	40	0.1	6.8	40	100	3	31
60	40	1	67.0	40	100	3.5	37.2
60	40	2	135.5	60	0	0.1	1.9
60	40	3	203.0	60	0	0.5	9.6
60	40	4	271.3	60	0	1	19.2
60	60	0.1	7.0	60	0	2	38.5
60	60	1	66.0	60	0	2.5	48.1
60	60	2	132.3	60	0	3	57.7
60	60	3	200.5	60	0	3.5	67.3
60	60	4	270.5	60	20	0.1	2.2
60	80	0.1	6.8	60	20	0.5	10.8
60	80	1	52.5	60	20	1	21.7
60	80	2	108.8	60	20	2	43.4
60	80	3	167.5	60	20	2.5	54.2
60	80	4	229.0	60	20	3	65.1
60	100	0.1	5.8	60	20	3.5	75.9
60	100	1	33.0	60	40	0.1	2.0
60	100	2	71.5	60	40	0.5	10.0
60	100	3	112.8	60	40	1	20.1
60	100	4	159.0	60	40	2	40.1
				60	40	2.5	50.1
				60	40	3	60.2
				60	40	3.5	70.2
				60	60	0.1	1.7
				60	60	0.5	8.4
				60	60	1	16.8
				60	60	2	33.6
				60	60	2.5	42.0
				60	60	3	50.3
				60	60	3.5	58.7
				60	80	0.1	1.3
				60	80	0.5	6.3
				60	80	1	12.7
				60	80	2	25.4
				60	80	2.5	31.7
				60	80	3	38.1
				60	80	3.5	44.4
				60	100	0.1	0.9
				60	100	0.5	4.5
				60	100	1	9.0
				60	100	2	18.0
				60	100	2.5	22.5
				60	100	3	27.0
				60	100	3.5	31.5

[a] 100 kPa = 1bar.

$$\hat{\eta}(x,\hat{T}) = (a_1 e^{a_2\hat{T}} + a_3)\cdot a_4(x-a_5)^2 \quad (8)$$

$$\hat{\eta}(x,\hat{T}) = a_4\hat{T}^{a_1}\cdot(x-a_2)^2 \quad (9)$$

$$\hat{\eta}(x,\hat{T}) = (a_1 e^{-a_2\hat{T}} + a_3)x^2 + (a_4 e^{-a_5\hat{T}} + a_6)x + (a_7 e^{-a_8\hat{T}} + a_9) \quad (10)$$

The transformations of T and $\eta(x, T)$ investigated systematically are summarized generally in Table 3. Each transformation in Table 3 represents a larger group of specific transformations tested. For example $\log(\eta)$ may be represented as $\log(\eta + c)$, $\log(b\eta)$, $\log(b\eta^N)$, or most generally as $\log(b\eta^N + c) + d$ where a, b, c, d, and N are coefficients that were varied to find an appropriate transformation, and $\eta°$ enables formally nondimensionalization of value one. Similarly, this approach was employed for temperature. The most general forms for the power function and the exponential function are $a\eta^N + b$ with $N \leq 1$ and $ae^{-bT} + c$, respectively. The transformations in viscosity and temperature were paired to calculate and assess the least-squares error for each expression. This systematic iterative testing involved, of the order of one hundred, sets of functions in coupled expressions to map the viscosity surface for MeOH−H_2O and ACN−H_2O as a function of composition and temperature.

By fixing one transformation in one variable, η, and varying the transformations in T, the order in which the least-squares

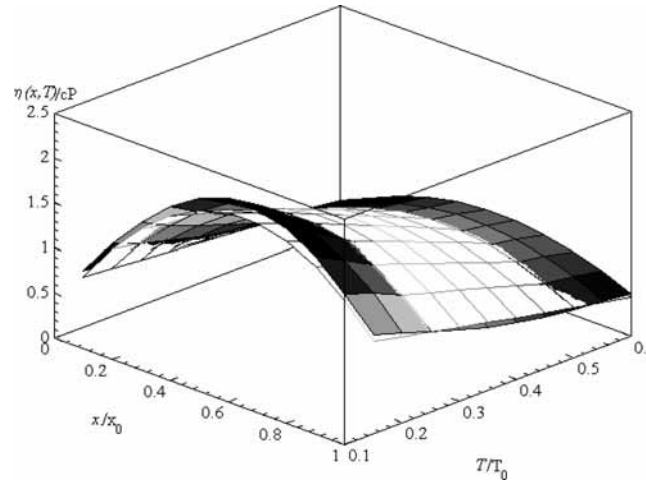

Figure 4. Viscosity surface function, MeOH−H_2O, eq 2 (□, fitted surface; ■, data), where $T_o = 10$ and $x_o = 100$.

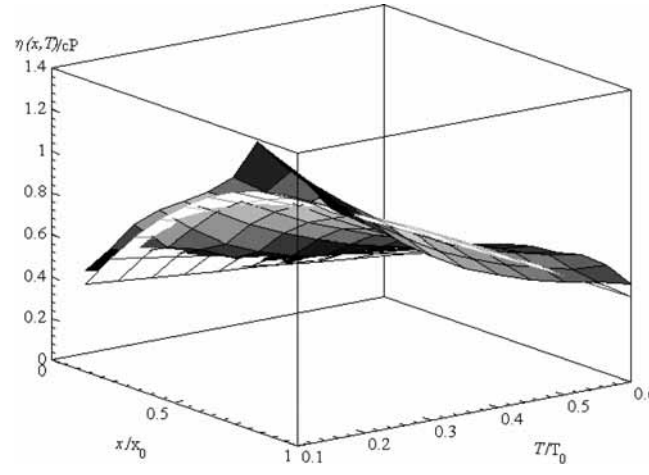

Figure 5. Viscosity surface function, ACN−H_2O, eq 2 (□, fitted surface; ■, data), where $T_o = 10$ and $x_o = 100$.

Table 3. Analysis of Viscosity Models as a Function of Temperature

equation	chemical	error	*A*	*B*	*C*	range K	
$\log(\eta) = A(1/T - 1/C)$	ACN[a]	0.9342	334.9	−	210.1	−	−
	ACN[c]	2.290E-4	1345	−	241.0	283	333
	MeOH[a]	0.6660	555.3	−	260.6	−	−
	MeOH[c]	1.000E-3	1443	−	264.7	283	333
$\log(\eta) = A + B/C - T$	ACN[b]	0.7124	−4.824	−430.4	13.17	280	360
	ACN[c]	2.685E-4	−3.222	−285.9	164.8	283	333
	MeOH[a]	0.7912	−1.681	−354.9	48.59	175	323
	MeOH[b]	0.6850	−2.297	−675.4	−33.89	248	333
	MeOH[c]	1.000E-3	−5.407	−1418	2.420	283	333

[a] Reid, Prausnitz, pp 637, 634, 454. [b] Viswanath, pp 163, 184. [c] Tarfulea.

Table 4. Errors: Nontransformed Equations

eq no.	MeOH	ACN
2	0.5823	0.3280
3	0.5942	0.3808
4	1.0695	0.4897
5	1.0061	0.4871

error decreases was found to be power, exponential, and logarithm. Similarly, applying this approach to temperature, *T*, the order in which the error decreases is logarithm and power. This analysis and findings are valid for both methanol and acetonitrile. In fact, the functions and transformations that reduce the error in methanol follow the same order of reduction for acetonitrile. The other functions tested besides those in eqs 2 to 9 made little difference in the error because of the nature of the smoothening of the transformed data. The errors calculated in applying eqs 6 to 9 to methanol and acetonitrile are summarized in Table 5 with their corresponding transformations.

Transformation (v) applied to eq 10 gave the lowest error. It is fortuitous that the transformed data and untransformed data both gave the minimum error with functions of the same form, eqs 2 and 10. Lastly, note that by transforming the data a reduction of more than 1 order of magnitude in the error was obtained. For MeOH−H_2O, the error reduced from 0.6 to 0.01, and for ACN−H_2O the error reduced from 0.3 to 0.008 for transformed and untransformed equations, respectively.

Figures 7 and 8 compare the fitted data with experimental data for MeOH−H_2O and ACN−H_2O, respectively. In both cases, the transformed shape has enabled a lower error. The

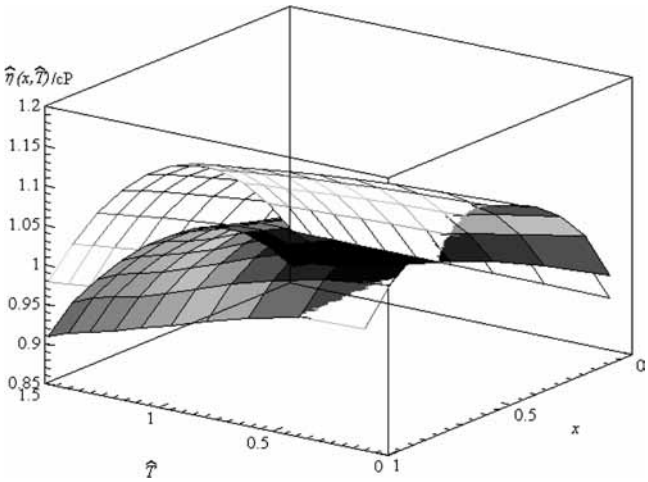

Figure 6. Viscosity surface: coupled product of exponent in *T* and quadratic in *x*, MeOH−H_2O, eq 2, transformation (v) (□, fitted surface; ■, data).

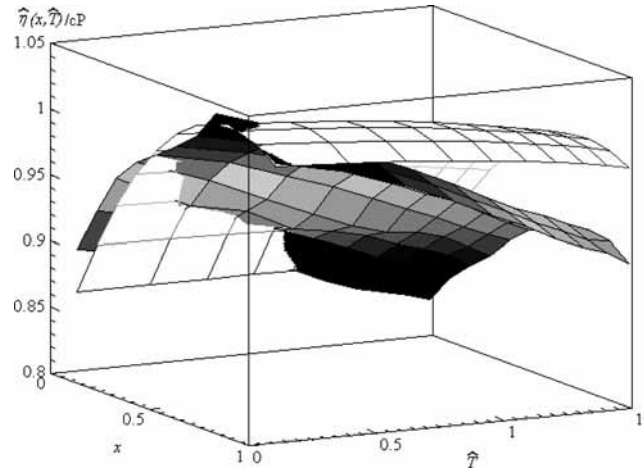

Figure 7. Viscosity surface: coupled product of exponent in *T* and quadratic in *x*, ACN−H_2O, eq 2, transformation (v) (□, fitted surface; ■, data).

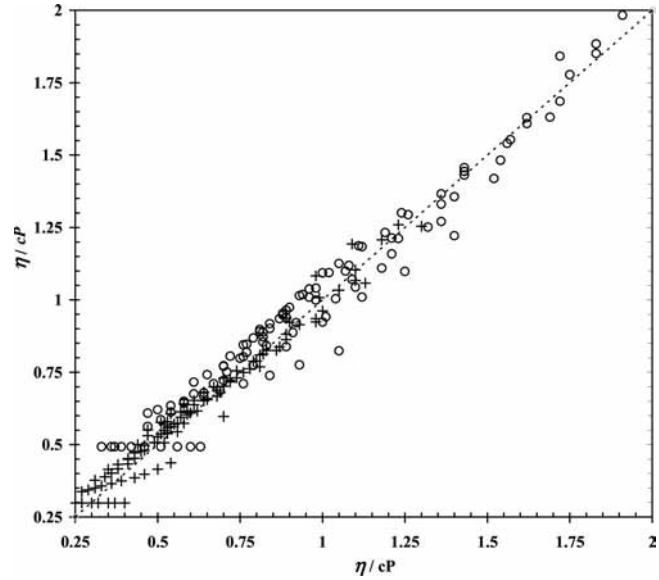

Figure 8. Calculated methanol−H_2O and acetonitrile−H_2O viscosity (eq 10, transformation (v)) versus the measured viscosity (+, ACN−transformed; ○, MeOH−transformed).

Table 5. List of Transformations or Mappings

viscosity	temperature
$\log(\eta)$	$\log(T)$
$\eta^{<1}$	$T^{<1}$
η	e^{-T}

z-axis scale for Figures 7 and 8 is small compared to the untransformed graphs in Figures 5 and 6. For methanol, the *z*-axis scale range for $\hat{\eta}$ is 0 to 1.2 corresponding to an untransformed scale in η of 0 to 2.5. Since the *z*-axis scale for $\hat{\eta}$ was reduced to 0.85 to 1.2, there is a visual magnification of the differences between these two surfaces compared to the untransformed graphs. Therefore, the quantitative analysis provided in Table 2 and Table 4 is required for comparison of the least-squares errors. Similarly, this interpretation applies to acetonitrile. The simplification of the viscosity surface via transformation to one that can be represented by the product or sum of elementary functions leads to reduced least-squares error. This is observed visually in the graphs as the transformed surfaces intersect the experimental surface once in contrast to the untransformed case where there are multiple intersections.

Table 5 summarizes the coefficients for eq 2 in the untransformed case and eq 10 in the transformed case, respectively,

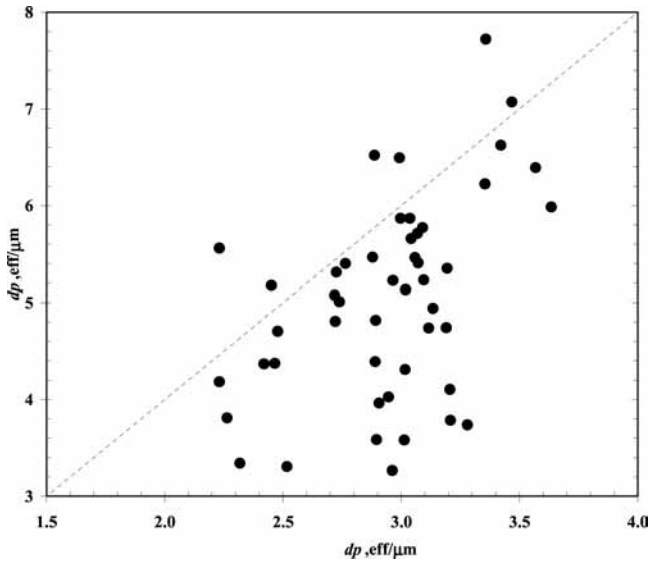

Figure 9. Effective particle size for methanol versus acetonitrile.

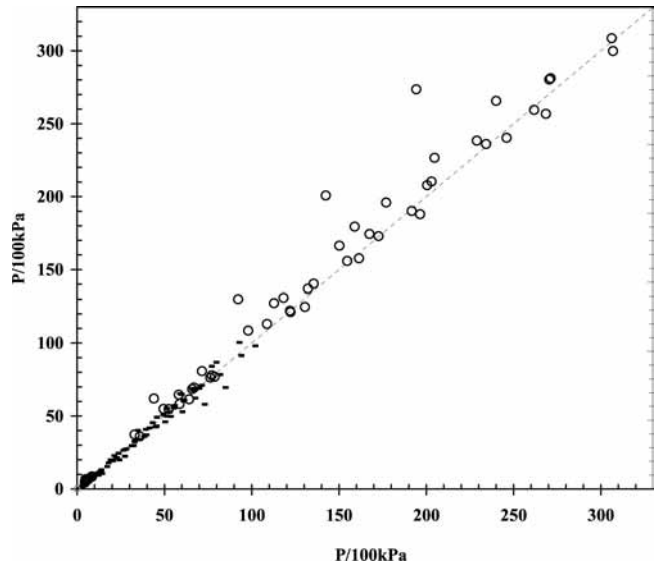

Figure 10. Measured pressure versus the calculated pressure for MeOH−H_2O and ACN−H_2O using transformed variables (−, ACN transformed; ○, MeOH transformed).

for MeOH−H_2O and ACN−H_2O. The coefficients a_2 and a_5 in the exponent of T or $\hat{T}$ and for eqs 2 and 10, respectively, are different in the transformed and untransformed cases within each solvent system. The coefficients of the quadratic in x are exponential functions of T, thus they have a significant impact on the shape of the surface. However, the coefficients a_3, a_6, and a_9 are similar with each solvent system in the transformed and untransformed cases as their role is to essentially translate the function of T or $\hat{T}$ with each solvent system and thus are similar in value.

IV. Application of Square Plots to Evaluate Measured and Calculated Results. Figure 8 illustrates the calculated viscosity based on the transformed function in eq 10 and the measured viscosity at each composition and temperature. The closeness of the symbols to the diagonal shows that the viscosity surface function, $\eta(x,T)$, for MeOH−H_2O and ACN−H_2O based on transformed data fits well the measured values. For MeOH−H_2O, the low viscosity range is not well predicted; however, for ACN−H_2O, the entire range of compositions and temperatures is fitted by the surface function in eq 10 and transformation (v).

The utility of a surface viscosity function is to predict the operating pressure drop as a function of composition and temperature for design calculations. To apply eq 1, the effective particle size is determined from the known pressure drop. The nominal particle size is not usually representative of the effective particle size even for virgin columns due to fines in the (2 to 3) μm range, an inherent consequence of the silica manufacturing process. Therefore, the experimental viscosity data and the measured pressure drop were utilized to determine the effective particle size at each composition and temperature for both ACN and MeOH. Figure 9 illustrates the effective particle size on the 5 μm column for the methanol data and the 10 μm column for the acetonitrile measurements. The pressure measurements made with methanol were determined on a 5 μm column as the blank pressure drop values were low. In contrast, the pressure measurements on the 10 μm column for acetonitrile were made close to the end of its life as the blank pressure drop values were high.

Figure 9 illustrates that the nominal 5 μm column has an average effective particle size of 3 μm with a percent relative standard deviation of 12 %. This lower value is primarily attributed to fines in the particles of the stationary phase. In contrast, the nominal 10 μm column has an average effective particle size of 5 μm with a percent relative standard deviation of 22 %. This difference is attributed to the measurements being made at the end of the column life due to a drop in the permeability of the frit. For these reasons, the data points in Figure 9 are mostly below the diagonal.

Table 6. Summary of Transformation-Mapping Combination Errors

label	$\hat{T}$	$\hat{\eta}$	error MeOH	error ACN
i	$T^{1/4}$	$\log(\eta)$	0.3734	0.2031
ii	$(T/T_o)^{1/4}$	$\log(\log(\eta)+1.5)$	0.0216	0.0308
iii	e^{-T}	$\eta^{1/4}$	0.0286	0.0413
iv	$\log(T)$	$\eta^{1/8}$	0.0115	0.0090
v	$\log(T)+2$	$\eta^{1/8}$	0.0106	0.0085

Table 7. Summary of Coefficients for Minimum Error

	untransformed, eq 2		transformed, eq 10	
coefficients	MeOH	ACN	MeOH	ACN
a_1	6.38	9.81	10.0	10.2
a_2	−0.784	−0.136	−0.0227	−0.0155
a_3	−11.4	−11.0	−10.6	−10.5
a_4	−9.78	−11.3	−11.8	−12.0
a_5	−0.609	−0.213	−0.0237	−0.0182
a_6	15.4	13.4	12.5	12.4
a_7	−0.868	−0.492	−0.000	−0.000
a_8	−0.536	−0.503	−7.87	−7.93
a_9	1.50	0.863	0.915	0.860

The analysis of the effective particle size allows the pressure drop to be calculated by evaluating only the effect of the viscosity function. The pressure drop was calculated using eq 1 and the viscosity values obtained from eq 10 using transformation (v) and the coefficients in Table 6 for both MeOH−H_2O and ACN−H_2O at each composition and temperature. Figure 10 illustrates a square plot of the calculated value of the pressure and the measured value of the pressure for both MeOH−H_2O and ACN−H_2O. In both cases, the data points follow the diagonal. For ACN−H_2O, the points overlay with the diagonal, while for MeOH−H_2O, an offset is observed suggesting a slightly higher calculated pressure than that measured.

The nonlinear effects of viscosity with the variation of both composition and temperature for methanol−water and aceto-

nitrile−water systems exhibit large nonlinearities for this critical system used in reversed-phase process chromatographic unit operations. These nonlinearities are a result of strong interactions from hydrogen bonding that vary with temperature and composition. A complex emperical equation has been determined to calculated the effect of both composition and temperature for design and safety considerations in chromatographic unit operations.

Conclusions

The viscosity as a function of composition and temperature at atmospheric pressure is highly nonlinear for aqueous methanol systems. The degree of nonlinearity is less for acetonitrile. The surface was fitted by interconnecting various elementary functions and tested in a systematic manner to fit the MeOH and ACN surfaces. Iteration by visual observation of the 3-D graphs and evaluation of the least-squares error were performed to find expressions giving a good fit. To reduce the error, transformation of the data using elementary functions was necessary to create a modified surface simpler in form. For MeOH−H_2O, the least-squares error was 0.6 and 0.01 for untransformed data and transformed data, respectively. Similarly, for ACN−H_2O the error was 0.3 and 0.008 for untransformed and transformed data, respectively.

The expression describing the viscosity−composition−temperature relationship for both the transformed and untransformed data was a quadratic in x with exponential functions of T as coefficients. The transformed temperature is $\log(T) + 2$, while the transformed viscosity was $\eta^{1/8}$.

Lastly, the closeness of the measured and calculated viscosity and pressure drop is exhibited in square plots with data points overlaying the diagonal.

Literature Cited

(1) Guiochon, G.; Felinger, A.; Shirazi, D.; Katti, A. *Fundamentals of Preparative and Liquid Chromatography*, 4th ed.; Elsevier-Academic Press: Amsterdam, 2006.

(2) Lee, K.; Mun, S.; Cauley, F.; Cox, G.; Wang, N-H. L. Optimal Standing-Wave Design of Nonlinear Simulated Moving Bed Systems for Enantioseparation. *Ind. Eng. Chem. Res.* **2006**, *45*, 739–752.

(3) Chin, C.; Xie, Y.; Alford, J.; Wang, N-H. L. Analysis of Zone and Pump Configurations in Simulated Moving Bed Purification of Insulin. *AIChE J.* **2006**, *52*, 2447–2460.

(4) Carta, G. JACS Book Reviews. *J. Am. Chem. Soc.* **2003**, *125*, 3398–3399.

(5) Chen, F.; Drumm, E.; Guiochon, G. Stress Distribution and Dimensional Changes in Chromatographic Columns. *J. Chromatogr.* **2005**, *1083*, 68–79.

(6) Mayfield, K.; Shalliker, R.; Catchpoole, H.; Sweeney, A.; Wong, V.; Guiochon, G. Viscous Fingering Induced Flow Instability in Multidimensional Liquid Chromatography. *J. Chromatogr.* **2005**, *1080*, 124–131.

(7) Katti, A.; Kmiotek, K.; Geng, J.; Goel, P. A Direct Approach to Insulin Isotherm Analysis in Reversed Phase Chromatography. *Chromatographia* **2007**, submitted.

(8) Neue, U.; Kele, M. Performance of Idealized Column Structures under High Pressure. *J. Chromatogr.* **2007**, *1157*, 236–244.

(9) Gritti, F.; Guiochon, G. Effect of the Flow Rate on the Measurement of Adsorption Data by Dynamic Frontal Analysis. *J. Chromatogr.* **2005**, *1069*, 31–42.

(10) Martin, C.; Coyne, J.; Carta, G. Properties and Performance of Novel High Resolution/High-Permeability Ion-Exchange Media for Protein Chromatography. *J. Chromatogr.* **2005**, *1069*, 43–52.

(11) Marchetti, N.; Guiochon, G. Separation of Peptides from Myoglobin EnzymaticDigests by RPLC. Influence of the Mobile-Phase Composition and the Pressure on the Retention and Separation. *Anal. Chem.* **2005**, *77*, 3425–3430.

(12) Golshan-Shirazi, S.; Guiochon, G. Optimization of experimental conditions in Preparative Liquid Chromatography Trade-Offs between Recovery Yield and Production Rate. *J. Chromatogr.* **1991**, *536*, 57–73.

(13) Ganetsos, G.; Barker P. *Preparative & Production Scale Chromatography*; Marcel Dekker: New York, 1993.

(14) Roman, J.; Abbott, E.; Xu, X.; Fox, S.; Veenstra, T.; Issaq, H. Optimization of Experimental Parameters for Packed Column Supercriticcal Fluid Chromatography. *J. Liq. Chromatogr.* **2007**, *30*, 2037–2044.

(15) García-Villar, N.; Saurina, J.; Hernández-Cassou, S. High-Performance Liquid Chromatographic Determination of Biogenic Amines in Wines with an Experimental Design Optimization Procedure. *Anal. Chim. Acta* **2006**, *575*, 97–105.

(16) Bounine, J.; Guiochon, G.; Colin, H. A Simple Pragmatic Optimization Procedure for some Parameters involved in High-Performance Liquid Chromatographic Separations: Column Design, Temperature, Solvent Flow-Rate and Composition. *J. Chromatogr.* **1984**, *298*, 1–20.

(17) Paredes, G.; Mazzotti, M. Optimization of Simulated Moving Bed and Column Chromatography for a Plasmid DNA Purification Step and for a Chiral Separation. *J. Chromatogr.* **2007**, *1142*, 56–68.

(18) Felinger, A.; Guiochon, G. Comparing the Optimum Performance of the Different Modes of Preparative Liquid Chromatography. *J. Chromatogr.* **1998**, *796*, 59–74.

(19) Felinger, A.; Guiochon, G. *Biotechnol. Prog.* **1996**, *12*, 638–644.

(20) Patel, K.; Jerkovich, A.; Link, J.; Jorgenson, J. In-Depth Characterization of Slurry Packed Capillary Columns with 1.0-um Nonporous Particles Using Reversed-Phase Isocratic Ultrahigh-Pressure Liquid Chromatography. *Anal. Chem.* **2004**, *76*, 5777–5786.

(21) Katti, A. Separation Methods in Drug Synthesis and Purification. *Handbook of Analytical Separations*; Valko, K., Ed.; Elsevier: Amsterdam, 2000; *Vol. 1*.

(22) Katti, A.; Jageland, P. Development and optimization of industrial scale chromatography for use in manufacturing. *Analusis* **1998**, *25*, 38–44.

(23) Rajendran, A.; Kräuchi, O.; Mazzotti, M.; Morbidelli, M. Effect of Pressure Drop on Solute Retention and Column Efficiency in Supercritical Fluid Chromatography. *J. Chromatogr.* **2005**, *1092*, 149–160.

(24) Fenghour, A.; Wakeham, W.; Vesovic, V. The Viscosity of Carbon Dioxide. *J. Phys. Chem. Ref. Data* **1998**, *27*, 31–45.

(25) Gritti, F.; Guiochon, G. Consequences of the Radial Heterogeneity of the ColumnTemperature at High Mobile Phase Velocity. *J. Chromatogr.* **2007**, *1166*, 47–60.

(26) Reid, R.; Prausnitz, J.; Poling, R. *The Properties of Gases & Liquids*, 4th ed.; McGraw-Hill: New York, 1987.

(27) Xiang, H.-W.; Laesecke, A.; Huber, M. A New Referece Correlation for the Viscosity of Methanol. *J. Phys. Chem. Ref. Data* **2006**, *35*, 1597–1621.

(28) Teske, V.; Vogel, E. Viscosity Measurements on Methanol Vapor and their Evaluation. *J. Chem. Eng. Data* **2006**, *51*, 628–635.

(29) Thompson, J.; Kaiser, T.; Jorgenson, J. Viscosity Measurements of Methanol-Water and Acetonitrile-Water Mixtures at Pressures up to 3500 bar using a Novel Capillary Time-of-Flight viscometer. *J. Chromatogr.* **2006**, *1134*, 201–209.

(30) Grunberg, L.; Nisson, A. Mixture Law for Viscosity. *Nature* **1949**, *164*, 799–800.

(31) Arrhenius, S. On the Dissociation of Substances Dissolved in Water [translated]. *Z. Phys. Chem.* **1887**, *1*, 631–648.

(32) Li, J.; Carr, P. Accuracy of Empirical Correlations for Estimating Diffusion Coefficients in Aqueous Organic Mixtures. *Anal. Chem.* **1997**, *69*, 2530–2536.

(33) González, B.; Calvar, N.; Gómez, E.; Domínguez, Á. Density, dynamic viscosity, and derived properties of binary mixtures of methanol or ethanol with water, ethyl acetate, and methyl acetate at T = (293.15, 298.15, and 303.15) K. *J. Chem. Thermodyn.* **2007**, *39*, 1578–1588.

(34) Teja, A.; Rice, P. Density, dynamic viscosity, and derived properties of binary mixtures of methanol or ethanol with water, ethyl acetate, and methyl acetate at T = (293.15, 298.15, and 303.15) K. Generalized Corresponding States Method for the Viscosities ofLiquid Mixtures. *Ind. Eng. Chem. Fundam.* **1981**, *20*, 77–81.

(35) Roy, M.; Sarkar, B.; Chanda, R. Viscosity, Density, and Speed of Sound for the Binary Mixtures of Formamide with 2-Methoxyethanol, Acetophenone, Acetonitrile, 1,2-Dimethoxyethane, and Dimethylsulfoxide at Different Temperatures. *J. Chem. Eng. Data* **2007**, *52*, 1630–1637.

(36) Herráez, J.; Belda, R. Viscous Synergy of Pure Monoalcohol Mixturesin Water and its Relation to Concentration. *J. Solution Chem* **2004**, *33*, 117–129.

(37) Viswanath, D.; Ghosh, T.; Prasad, D.; Dutt, N.; Rani, K. *Viscosity of Liquids*; Springer: Amsterdam, 2007.

(38) Jacobson, S.; Felinger, A.; Guiochon, G. *Biotechnol. Prog.* **1992**, *8*, 533–539.

(39) Kaplan, W. *Advanced Calculus*, 2nd ed.; Addison-Wesley: Reading, MA, 1973.

(40) Varberg, D.; Purcell, E.; Rigdon, S. *Calculus Early Transcendentals*; Pearson-Prentice Hall: Upper Saddle River, NJ, 2007.
(41) Katti, A.; Hopper C.; Tarfulea, N. E. Experimental and Empirical Characterization of Reversed Phase Media. *J. Liq. Chromatogr.* **2007**, accepted.
(42) Colin, H.; Diez-Masa, J.; Czaykowska, T.; Miedziak, I.; Guiochon, G. The Role of the Temperature in Reversed-Phase High Performance Liquid Chromatography using Pyrocarbon Containing Adsorbents. *J. Chromatogr.* **1978**, *167*, 41–65.
(43) Nelder, J.; Mead, R. A simplex method for function minimization. *Comput. J.* **1965**, *7*, 308–313.

Received for review August 2, 2008. Accepted September 18, 2008. The authors thank the support of Daiso Corporation for sponsoring this work, Purdue University Grant No. 202435. In addition, the authors thank Purdue University Calumet programs for the Louis Stokes Alliance for Minority Participation Award (LSAMP), the Office of Research and Professional Development, the Student Research Office, the Undergraduate Research Grant Program (URGP), and the Student-Faculty Research Collaboration Award (SFRCA) for support of this research.

JE800607J